RSC Advances




ROYAL SOCIETY OF CHEMISTRY

www.rsc.org/advances

# Novel Graphene Oxide Sponge synthesized by Freeze-Drying Process for the Removal of 2,4,6-Trichlorophenol

Jiali WANG[1,2], Xueli GAO[1,2,*], Yuhong Wang[3], Congjie GAO[1,2]

1. Key Laboratory of Marine Chemistry Theory and Technology, Ministry of Education, Ocean University of China, Qingdao 266100, China

2. College of Chemistry and Chemical Engineering, Ocean University of China, Qingdao 266100, China

3. National Center of Ocean Standards and Metrology, Tianjin 300112, China

*Corresponding author; Tel/Fax.: +86-532-66782017;

Email address:wangjialiouc@gmail.com; gxl_ouc@126.com

## Abstract:

Graphene oxide (GO) spongy materials as environmental pollutant scavengers have drawn great attentions owing to ultralarge surface area, unique spongy structure and hydrogen-bonding interactions. Herein, novel GO sponge was synthesized by improved Hummer's method followed freeze-drying process and its adsorption capacity of 2,4,6-trichlorophenol (TCP) was investigated. The structural features of GO sheets and GO sponge have been characterized by Fourier transform infrared spectroscopy (FTIR), X-ray diffraction (XRD), Raman spectroscopy, X-ray photoelectron spectroscopy (XPS), atomic force microscope (AFM) and scanning electron microscopy (SEM). Specific surface area assessment and pore distribution measurements were analyzed by Micromeritics ASAP 2020. Adsorption mechanism and kinetic study of TCP on GO sheets and GO sponge were researched using a batch equilibration method. The results suggest that GO sponge presented higher adsorption capacity than GO sheets due to large specific surface areas and TCP had optimum adsorption capacity on both GO sheets and GO sponge at pH 2.0~6.0. Adsorption isotherms and kinetics curves of TCP on GO sheets and GO sponge were nonlinear, indicating the homogeneous monolayer chemical adsorption.


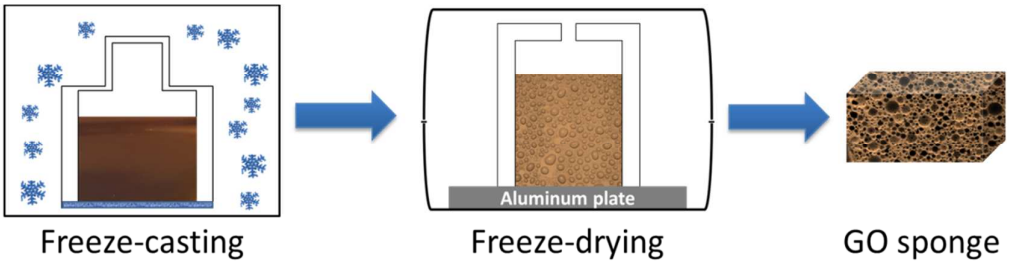


**Keywords:** graphene oxide, freeze-drying, 2,4,6-trichlorophenol, adsorption

## 1. Introduction

Hazardous persistent aromatic materials produced by pharmaceutical, petrochemical, dyestuff, pesticide, and other industries have been a severe environmental concern. 2,4,6-Trichlorophenol (TCP) is a very common pollutant in the aquatic environment due to its toxicity, stability, and bioaccumulation[1]. Discharge of TCP-contaminated wastewater into aquatic environment without adequate treatment can pose adverse effects on human nervous system and cause many health disorders [2]. Numerous studies focused on the efficient removal of TCP from aqueous solutions such as by photocatalysis[3], adsorption[4], and electrolysis[5]. Due to the structural stability and persistence of TCP in the environment, adsorption has been found to be superior to other techniques as a result of its low-cost, high efficiency and easy operation.

Graphene (GN) is a two-dimensional structure consisting of $sp^2$ hybridized carbons with only one atomic thickness, and has attracted significant attentions since its discovery[6]. Graphene oxide (GO) is a highly oxidized form of chemically modified GN that consists of single-atom-thick layer of GN sheets with carboxylic acid, epoxide and hydroxyl groups in the plane[7]. Due to its atomic-level thickness, large theoretical specific surface area, remarkable electronic and chemical properties, potential environmental applications of GO as superior adsorbent have been recognized for the removal of organic contaminants and metal ions in water. Gao et al.[8] revealed the high adsorption of tetracycline antibiotics on GO. Lin et al.[9] found that arginine-capped iron oxide/rGO nanocomposite is effective adsorbents for acid

dye removal. In addition, GO also have high adsorption affinity for heavy metals, where the amount of active surface sites on GO is an important factor influencing the adsorption of heavy metal ions. Previous works on Cd(II) and Co(II) adsorption onto few-layered GO nanosheets[10], and on Hg(II) adsorption to polypyrrole-reduced GO composites[11] showed that GO composites have a strong adsorption affinity for metal ions.

Spongy GN and GO materials are applied as environmental pollutant adsorbents by utilizing the characteristics of ultralarge surface area, electrostatic interactions or hydrogen bonds of oxygen-containing functional groups and strong π–π interaction on the surface[12-14]. Spongy graphene (SG) has been made by reducing graphene oxide platelets in suspension followed by shaping via moulding and heating and shows highly efficient absorption of not only petroleum products and fats, but also toxic solvents such as toluene and chloroform[15]. Liu et al.[16] generated a three dimensional (3D) graphene oxide sponge from a GO suspension through a simple centrifugal vacuum evaporation method, and used them to remove both the methylene blue (MB) and methyl violet (MV) dyes.

Nowadays, there are many forming processes following colloidal suspension to prepare spongy absorbing materials, such as slip casting, tape casting, screen printing, centrifugal vacuum evaporation[17-19]. The common issues for these techniques are the high fugitive organic contents and the problematic drying process because of the presence of capillary force; the high organic content poses challenges in the removal process, increases processing cost, and produces environmental hazards; the capillary

force generates drying stress and subsequently warping and cracking. However, freeze-drying process is a simple technique to produce porous complex-shaped inorganic composites or polymeric parts[20]. It provides materials with a unique porous structure, where the porosity is almost a direct replica of the frozen solvent crystals. Proper control of the freezing conditions yields materials with elongated and continuous porosity along the solidification direction. This unique structure endow materials with excellent compressive strength, open porosity, high pore connectivity, specific surface area and high adsorption ability[21]. Sun et al.[22] fabricated the hydrophobic CNT-GN aerogels by freeze-drying process and chemical reduction and the aerogels possess ultrahigh oil-absorption capacity. Furthermore, freeze-drying prevents defect formation by eliminating capillary force during drying and saves tremendous effort in binder removal and also has the advantage of little cost and facile utilization of non-toxic dispersing medium, such as water[23]. As a result, a shape-mouldable and nanoporous GO sponge is promisingly designed through freeze-drying as a versatile and effective sorbent material.

In this work, we have demonstrated that the application of GO sponge materials as environmental pollutant scavengers by utilizing unique porous structure with ultralarge surface area, electrostatic interactions or hydrogen bonds of oxygen-containing functional groups and π–π interaction on the surface. We prepared GO sheets using improved Hummer's method and generated GO sponge from GO suspension through freeze-drying process, and explored the potential application of GO sponge to remove TCP. The structural features of GO sheets and GO sponge have

been characterized by Fourier transform infrared spectroscopy (FTIR), X-ray diffraction (XRD), Raman spectroscopy, X-ray photoelectron spectroscopy (XPS), Atomic Force Microscope (AFM) and scanning electron microscopy (SEM). Kinetic study and adsorption mechanism on TCP adsorption were also investigated.

## 2. Materials and methods

### 2.1 Materials

Graphite was purchased from Bay Carbon. $H_2SO_4$ (95 wt. %) and $KMnO_4$ were all analytical grades and obtained from Beijing Chemical Works. $H_3PO_4$ (85 wt. %) was analytical grade and supplied by Nanjing Chemical Reagent Co., Ltd. $H_2O_2$ (30 wt. %) and HCl (36~38 wt. %) was analytical grade and obtained from Sinopharm Chemical Reagent Co., Ltd. TCP (97.4 wt. %) was purchased from Shanghai Zhenpin Chemical Co., Ltd. NaOH and $HNO_3$ (98 wt. %) were analytical grade and obtained from Sinopharm Chemical Reagent Co., Ltd. Methanol was HPLC grade and obtained from Merck Chemicals (Shanghai) Co., Ltd.

### 2.2 Synthesis of GO

GO was synthesized from graphite powder according to the improved Hummer's method [24] which is outlined in **Scheme 1**. The mixture of concentrated $H_2SO_4$/$H_3PO_4$ (90:10 mL) was added to a mixture of graphite flakes (1.0 g) and $KMnO_4$ (6.0 g). The reaction was then heated to 50 °C and stirred for 12 h. The reaction was cooled to room temperature and poured onto ice (~400 mL) with 30% $H_2O_2$ (10 mL). After

cooling, the mixture were centrifuged (7000 rpm for 4 h), and the supernatant was decanted away. The remaining solid material was then washed in succession with 200 mL of water, 200 mL of 30% HCl solution. The products obtained by centrifugation were vacuum-dried overnight at room temperature.

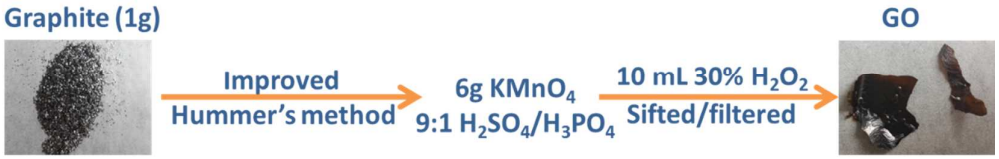


**Scheme 1** Synthesis of GO sheets

### 2.3 Preparation of GO sponge via freeze dry method

GO was re-dissolved in deionized water and ultrasonicated for 1 h at 200 W. The dispersion was centrifuged at 7000 rpm, and GO dispersion was obtained by discarding the precipitate. GO dispersion was placed on a metal die, which was then transferred to a cold source with constant temperature. Freezing lasted for 2h until the suspension was fully solidified. Temperatures above -50℃ can be achieved directly by applying cold traps to the FD-1A-80 freeze dryer (Boyikang corp., China). After GO were completely frozen, the samples were placed in a freeze dryer for 48 h, generating black GO sponges (**Scheme 2**).

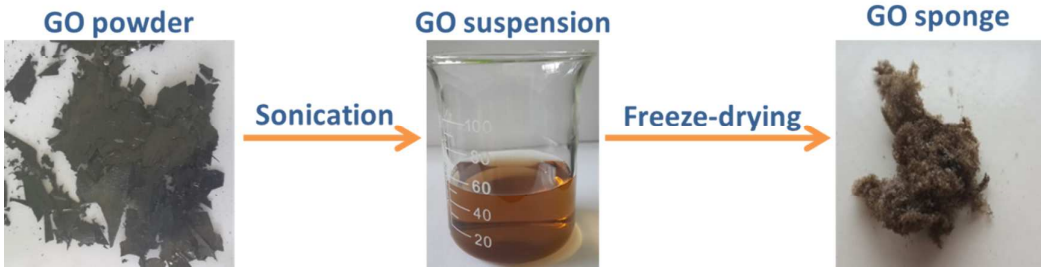


**Scheme 2** Preparation of GO sponges

### 2.4 Characterization of GO sheets and GO sponge

The Fourier transform infrared (FTIR) spectroscopy was performed using Tensor 27 spectrometer (Bruker, Germany) using the KBr pellet method at transmission reflectance (TR) mode. The FTIR spectra were scanned in the wavenumbers range from 650 to 4000 $cm^{-1}$ during 64 scans, with 2 $cm^{-1}$ resolution. X-ray powder diffraction (XRD) patterns were recorded using D8 ADVANCE diffractometer (Bruker, Germany), equipped with a Cu Kα radiation source (λ= 1.5418 Å). Raman scattering was performed on NEXUS 670 Microscopy (Thermo Nicolet, USA) with an excitation laser of 532 nm. The X-ray photoelectron spectroscopy (XPS) measurement was performed on ESCALAB 250 spectrophotometer (Thermo Fisher SCIENTIFIC, USA) with an achromatic Mg/Al X-ray source at 450W. Atomic force microscopy (AFM) images were recorded using Multimode-V microscope (Veeco, USA) in contact mode. AFM samples were prepared by drop casting the GO suspension in water onto freshly cleaved mica surfaces and dried under room temperature. The morphologies of GO sheets and GO sponge were observed using S-4800 scanning electron microscopy (SEM) (Hitachi, Japan) at a 15 kV accelerating voltage. The samples were coated with gold under an argon purge before the characterization. Specific surface area assessment and pore distribution measurements were carried out by $N_2$ adsorption-desorption analysis at 77 K using ASAP 2020 (Micromeritics, USA).

**2.5 Adsorption experiments of TCP on GO sheets and GO sponge**

**2.5.1 Effect of initial solution pH**

Batch adsorption experiments were carried out by using the GO sheets and GO

sponge as the adsorbents. All batch adsorption experiments were performed in triplicates on a SHA-C shaker (Changzhou, China) with a shaking speed of 150 rpm until the system reached equilibrium. 0.015 g of GO sheets was firstly dispersed in 15 mL of water and ultrasonicated for 15 min at 200 W for full suspension of GO. The pH effect experiments were respectively conducted by mixing 0.015 g of GO sponge or 15 mL of GO suspension with TCP into 30 mL mixture solution. The initial concentrations of TCP is 5.0 $mg \cdot L^{-1}$. After equilibrium was reached, the suspension was centrifuged at 5000 rpm for 15 min to separate liquid from solid phases, and the concentrations of solutes in the supernatant phase were determined by HPLC (LC-2010HT, Shimadzu, Japan). Controls were also prepared identically in triplicate but contained no adsorbents, which were simultaneously run to assess loss of solutes. Results showed that no significant loss of solutes was observed, indicating that microbial degradation, volatilization, or adsorption to the glass walls were negligible during the adsorption experiments. The adsorbed mass was calculated from the differences between the initial and final equilibrium concentrations, according to the following equation:

$$Q = \frac{(C_0 - C_e)V}{m} \quad (1)$$

where $C_0$ is the initial TCP concentration ($mg \cdot L^{-1}$), $C_e$ is the TCP equilibrium concentration ($mg \cdot L^{-1}$), V is the volume of TCP solution (L), and m is the mass of GO sheets and GO sponge (g).

**2.5.2 Adsorption equilibrium study**

Adsorption of TCP (1.0, 2.0, 5.0, 10.0, 15.0 and 20.0 $mg \cdot L^{-1}$) were carried out

using a batch adsorption approach as mentioned below. The suspended solution pH was adjusted to 5.0 ± 0.1 by addition of 0.1 M $HNO_3$ or 0.1 M NaOH. After equilibrium was reached, the initial and final TCP concentrations was detected by HPLC and the uptake was calculated based on Eq. (1) as mentioned above.

### 2.5.3 Adsorption kinetics study

Adsorption kinetics study on GO sponge or GO suspension was carried out with the initial TCP concentration of 10.0 mg·$L^{-1}$ at 298 K and pH 5.0 as mentioned above, respectively. About 1.0 mL of the solution was then taken out at desired time intervals to analyze the current TCP concentration. Meanwhile, the same volume of pure water was added into the bulk solution to keep the volume constant. The uptake at time $t_i$, $q(t_i)$ (mg·$g^{-1}$) was calculated using the following equation:

$$q(t_i) = \frac{(C_0 - C_{t_i})V_0 - \sum_2^{i-1} C_{t_{i-1}} V_s}{m} \quad (2)$$

where $C_0$ is the initial concentration of TCP (mg·$L^{-1}$) and $Ct_i$ is the TCP concentration at time $t_i$ (mg·$L^{-1}$). $V_0$ is the volume of the mixed solution (L) and $V_s$ is the volume of the sample solution taken out each time for TCP concentration analysis (L). In this equation, $V_s$ is equal to 1.0 mL. Finally, m represents the mass of the adsorbent (g).

## 3. Results and discussion

### 3.1 Characterization of GO sheets and GO sponge

The FTIR spectra of GO was shown in **Fig. 1**. The peak at 1620 $cm^{-1}$ was corresponding to C=C stretching vibration of the $sp^2$ carbon skeletal network. Oxygen-containing functional groups such as COOH (1730 $cm^{-1}$), C–OH (1400, 1240

$cm^{-1}$) and C–O–C (1050 $cm^{-1}$) were clearly visible. XRD pattern of GO was recorded in **Fig. 2**. The feature diffraction peak of GO at 11.107° was observed as the AB stacking order with layer-to-layer distance (d-spacing) of 7.959 nm. Compared with graphite (0.341nm, 2θ=26.08°)[7], the layer-to-layer distance of GO was larger because of the functional groups (such as epoxy and hydroxyl groups) on basal plane of GO sheet and the intercalated water molecules between layers. The Raman spectra of GO was presented in **Fig. 3**. The D-band at 1350 $cm^{-1}$ is related to the order/disorder degree from a breathing κ-point phonon of $A_{1g}$ symmetry and the G-band at 1595 $cm^{-1}$, which is an indicator of the stacking structure, is assigned to the $E_{2g}$ phonon of $sp^2$ hybridized carbon atoms[25]. The general Raman spectrum of graphite is demonstrated to have a strong G peak at 1570 $cm^{-1}$ [26]. Upon oxidation of graphite, the G-band was shifted toward longer wavenumber due to the formation of GO with oxygenated functional groups on its basal plane and at the edges. Besides, the $I_D/I_G$ ratio of GO was 0.939, which indicated $sp^2$ hybridized carbons were converted to $sp^3$ hybridized carbons due to generation of -OH, -COOH and epoxide groups during oxidation[27, 28]. **Fig. 4** showed the XPS spectra of GO. The C1s spectrum could be deconvoluted into three peak components with binding energies at 284.6, 286.0 and 288.5 eV, attributed to C-C, C-O and C=O species, respectively[29]. The XPS data in **Fig. 4(A)** showed that about 48.81% of carbon was not oxidized, 41.66% had C-O bond (representing hydroxyl and epoxide groups), 9.54% had COOH bond, and the O/C ratio was 0.61. The AFM image and its corresponding height profile were presented in **Fig. 5**. GO shows a height of around 0.737 nm, suggesting a single-layer nanosheet. The

microscopic topographies of GO sheets and GO sponge were analyzed using SEM and shown in **Fig. 6**. Changes were obvious in the SEM images of GO sheets and GO sponge. The GO sheets presented the sheet-like structure (**Fig. 6A**), while GO sponge presented spongy and foam-like structure owing to freeze-drying process (**Fig. 6B**). Thus, the results of FTIR, XRD, Raman spectroscopy, XPS, AFM measurements strongly prove the successful preparation of GO and SEM demonstrates the unique structure of GO sponge compared with GO sheets.

The porous property of GO sheets and GO sponge was investigated by nitrogen adsorption-desorption tests in **Fig. 7**. The adsorption/desorption isotherms both showed a characteristic H4 hysteresis loop, indicating the presence of mesopores. The surface area of GO sheets was 60 $m^2 \cdot g^{-1}$ by fitting the isotherms to the Brunauer-Emmett-Teller (BET) model, which were comparable to some reported works [30], while that of GO sponge was 189 $m^2 \cdot g^{-1}$. Therefore, GO sponge presented the remarkable higher surface area than GO sheets. The pore size distribution curves determined by the Barrett–Joyner–Halenda (BJH) method suggested that much of the pore volume of GO sheets and GO sponge lay in the pores with a diameter of 3.3–100 nm. The pore size distribution curve of GO sheets showed one sharp peaks at 3.7 nm, whereas that of GO sponge displayed a sharp peak at 3.8 nm and a broad peak at 16.4 nm. In addition, the pore volumes of GO sheets and GO sponge were 0.392 and 0.683 $cm^3 \cdot g^{-1}$, respectively. Overall, the pore size analyses are consistent with the SEM measurements, and all the results implied that GO sponge possessed ultralarge surface area and higher porosity.

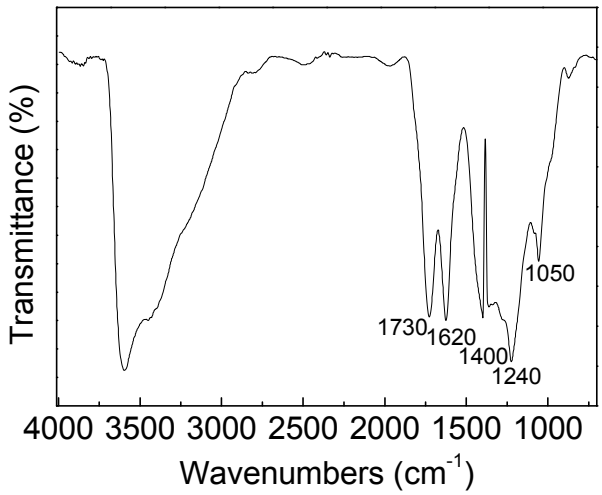


**Fig. 1** FTIR spectra of GO

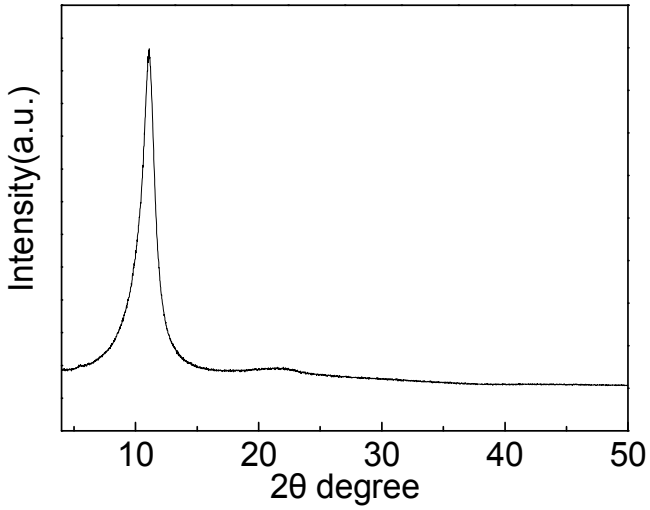


**Fig. 2** XRD spectra of GO

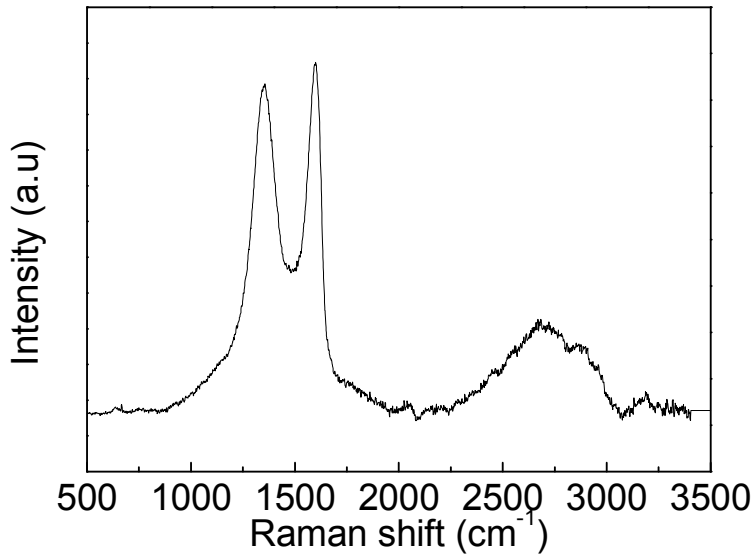


**Fig. 3** Raman spectra of GO

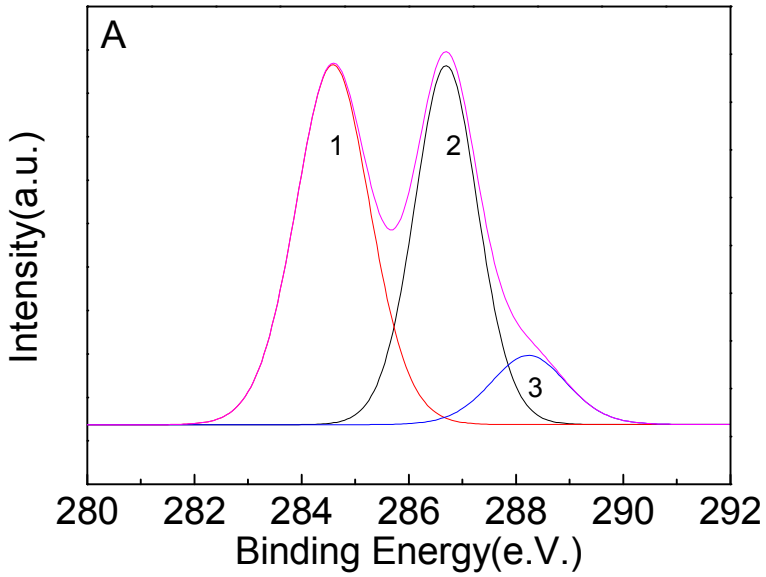

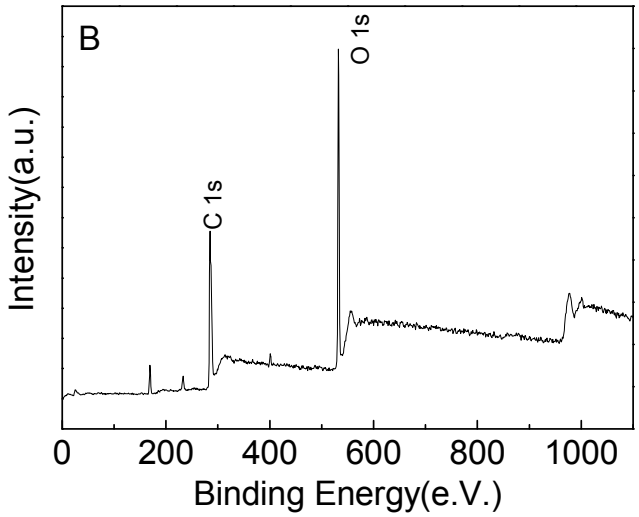


**Fig. 4** C1s XPS spectrum (A) and full survey (B) of GO

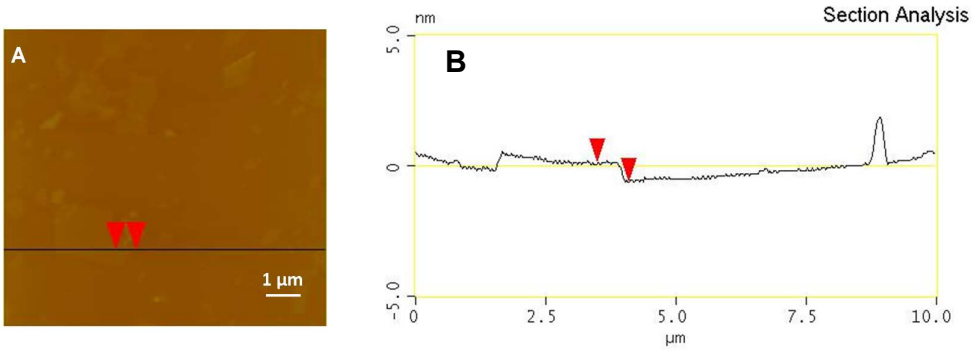


**Fig.5** AFM image (A) and height profile (B) of a single layer of GO

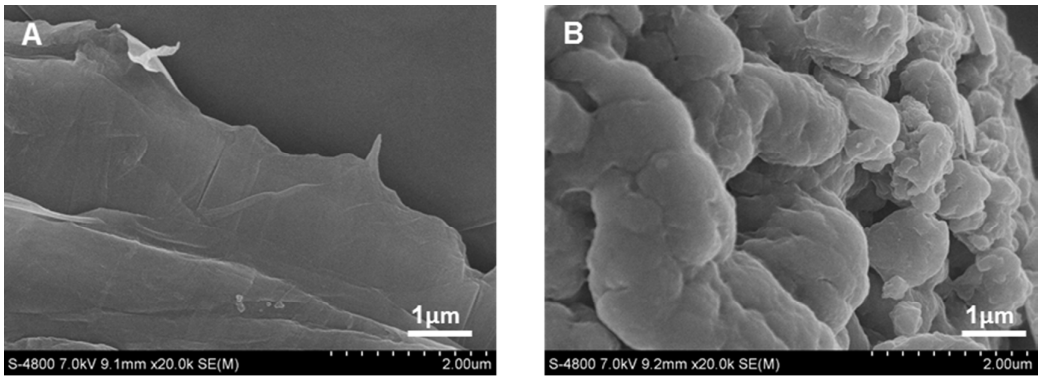


**Fig. 6** SEM images of GO sheets (A) and GO sponge (B)

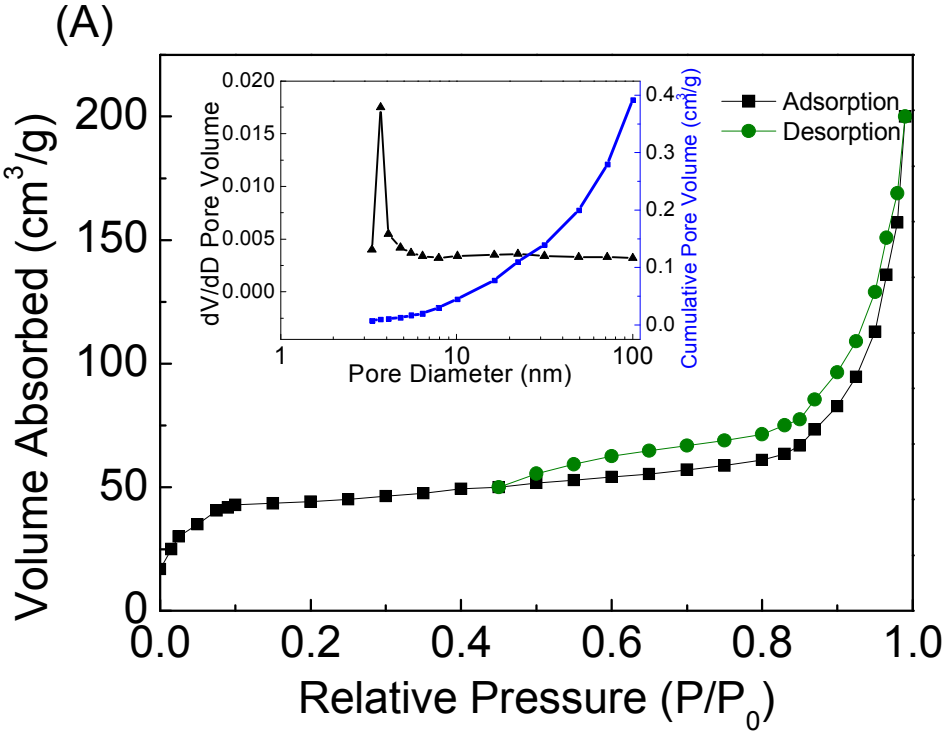


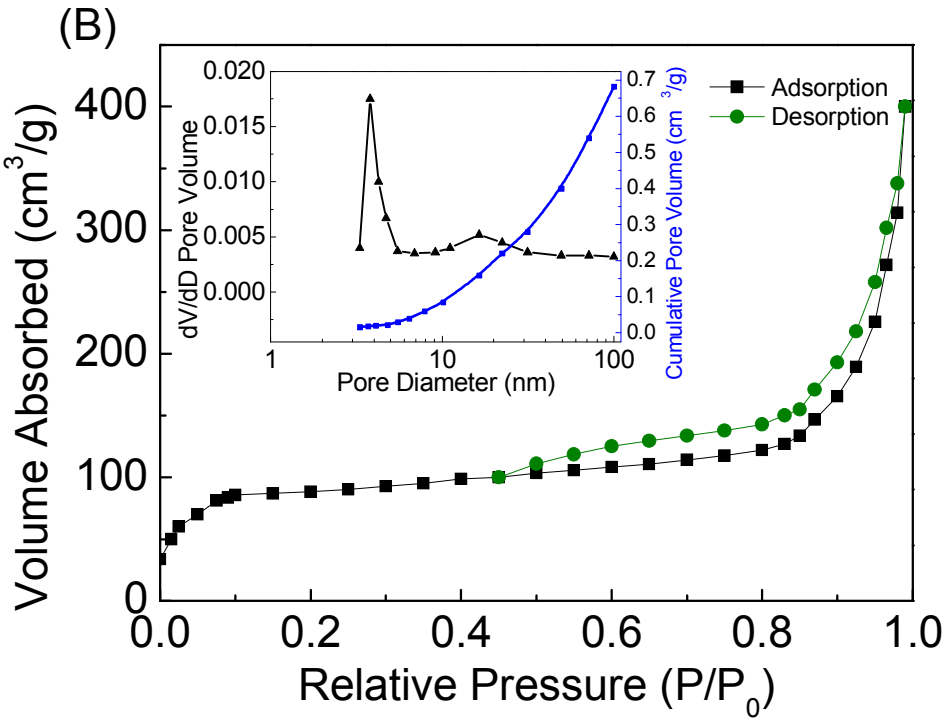


**Fig. 7** $N_2$ adsorption-desorption isotherms and pore size distribution curves (inset) of GO sheets (A) and GO sponge (B)

### 3.2 Adsorption study

#### 3.2.1 Effect of pH on adsorption

The pH of aqueous solution was an important parameter that determined the adsorption capacity and the results were illustrated in **Fig. 8**. The adsorption of TCP on both GO sheets and GO sponge decreased slightly over pH 2.0–6.0, decreased rapidly at pH>6.0 and then decreased slightly, consistent to the previous study on adsorption of TCP[31]. Considering pKa value of TCP (6.15), it appears that the greater adsorption at low pH may be due to higher content of neutral TCP. An increase in solution pH increased the fraction of negatively charged TCP, rendering the decrease of TCP adsorption. Besisdes, the introduction of many oxygen-containing groups endow GO with negative charges. Some of the anionic groups would be deprotonized at higher pH resulting in enhanced negative charge. Thus, electrostatic repulsion of anionic TCP with negatively charged surfaces of GO makes adsorption unfavorable. Therefore, the optimum pH range for TCP adsorption onto GO sheets and GO sponge adsorbents was 2.0-6.0.

GO sheets and GO sponge both have good adsorption capacity for TCP because the oxygen-containing functional groups of GO are facile to bind TCP due to electrostatic interactions or hydrogen bonds, and the aromatic matrix of GO tends to TCP by π-π stacking interactions[32]. However, the adsorption of TCP on GO sponge was almost twice higher than that of GO sheets, which may be resultant from its spongy structure. GO sponge has ultralarge surface area and high porosity due to porous structure, which has been already observed directly under SEM as mentioned

above. Therefore, GO sponge could be more facile to form parallel π-π stacking interactions with TCP in water and provides more inner interplanar sites for electrostatic or hydrogen-bonding interactions. The large adsorption area of GO sponge has thus effectively improved the TCP adsorption.

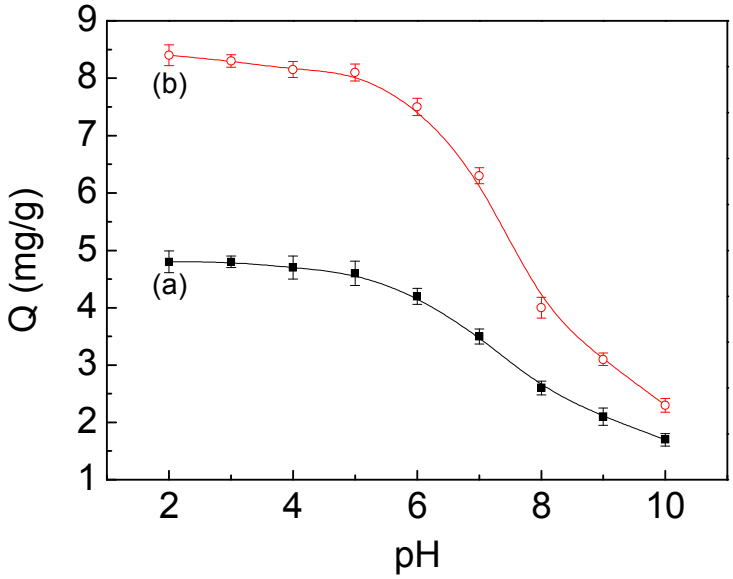


**Fig. 8** Effect of pH on the adsorption of TCP on GO sheets (a) and GO sponge (b)

### 3.2.1 Adsorption isotherms

The adsorption isotherms of the GO sheets and GO sponge for TCP were presented in **Fig. 9** and the isotherms fitting parameters were listed in **Table 1**. The equilibrium data were fitted by Langmuir and Freundlich and the equations are given below:

$$\frac{1}{Q_e} = \frac{1}{Q_m} + \frac{1}{K_1 Q_m C_e} \quad (3)$$

$$\ln Q_e = \frac{\ln C_e}{n} + \log k_f \quad (4)$$

where $Q_m$ is the theoretical maximum adsorption capacity per unit weight of the

adsorbent ($mg \cdot g^{-1}$), $K_f$ and $K_f$ are adsorption constants of Langmuir and Freundlich models ($L \cdot mg^{-1}$), respectively, and n is the Freundlich linearity index.

From **Fig. 9**, TCP uptakes of the GO sheets and GO sponge increased nonlinearly with increasing the initial TCP concentrations and both isotherms of GO sheets and GO sponge fitted Freundlich equation well. Interestingly, the TCP uptake of GO sponge was much more than that of GO sheets. It reveals that the adsorption sites on GO sponge with higher specific surface areas are sufficient and have strong interactions with TCP. The adsorption capacity relies on the amount of TCP transported from the bulk solution to the surfaces of the adsorbent at lower initial concentrations. The isothermal adsorption behavior of GO sheets and GO sponge both obey Freundlich equation, which reveals that a homogeneous monolayer adsorption is dominant in both GO sheets and GO sponge. Based on previous literatures, GN binding to adsorbates through parallel π-π stacking interactions usually forms multilayer adsorption[32]. However, π-π stacking interaction was not likely a primary cause of TCP adsorption on GO sheets and GO sponge. GO dominantly show monolayer adsorption because oxygen-containing functional groups of GO are facile to bind TCP due to electrostatic interactions or hydrogen bonds.

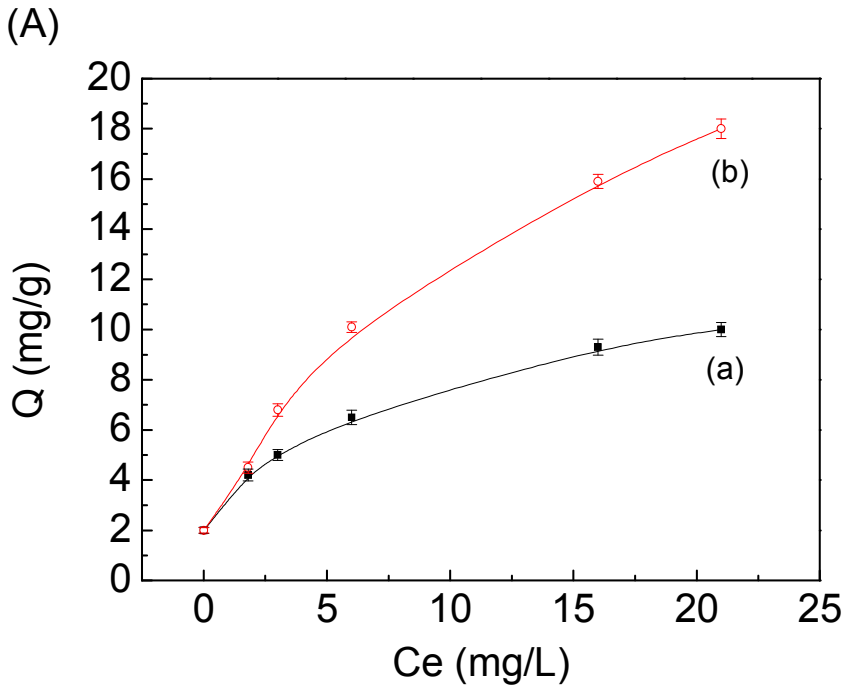


1

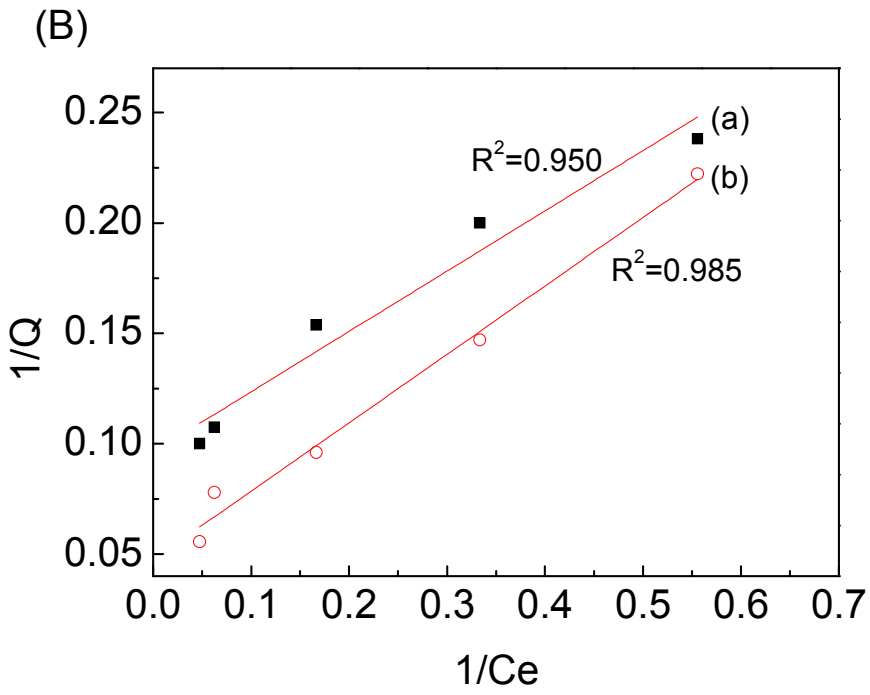


2

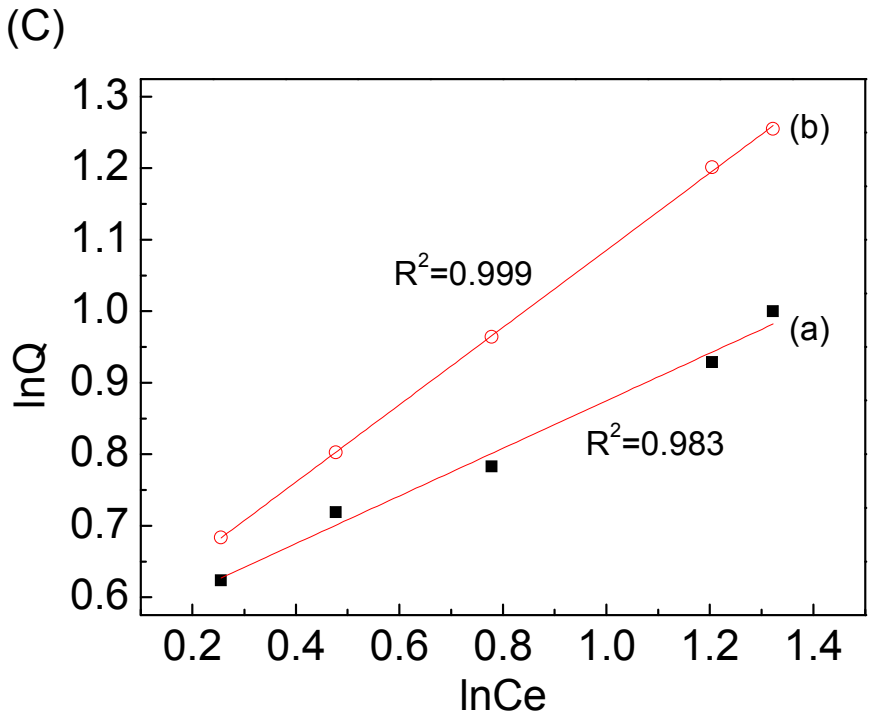


**Fig. 9** (A) Adsorption isotherms, (B) Langmuir and (C) Freundlich model fitting for TCP on GO sheets (a) and GO sponge (b)

| Adsorbents | Langmuir | | | Freundlich | | |
|---|---|---|---|---|---|---|
| | $Q_m$ (mg•g$^{-1}$) | $K_l$ (L•mg$^{-1}$) | $R^2$ | $K_f$ (L•mg$^{-1}$) | n | $R^2$ |
| GO sheets | 10.39 | 0.352 | 0.950 | 3.38 | 2.738 | 0.983 |
| GO sponge | 21.06 | 0.153 | 0.985 | 3.89 | 2.97 | 0.999 |

**Table 1** Langmiur and Freundlich adsorption isotherms fitting parameters of TCP on GO sheets and GO sponge

### 3.2.3 Adsorption kinetics

Aside from the adsorption equilibrium study, adsorption kinetics was also carried out to establish the time course of TCP uptakes on GO sheets and GO sponge. The typical experimental results of TCP adsorption versus time are shown in **Fig. 10**. The

adsorption at medium and low initial concentration achieved equilibrium in a short term, and reached a plateau at adsorption time of 30 min for GO sheets and 12 min for GO sponges, respectively. To further discuss the adsorption mechanisms, pseudo-first and pseudo-second order models were applied to study the experimental data. The non-linear forms of aforementioned kinetics models are presented below, respectively:

$$ln(Q_e - Q_t) = \ln Q_e - k_1 t \quad (4)$$

$$\frac{t}{Q_t} = \frac{1}{k_2 Q_e^2} + (\frac{1}{Q_e})t \quad (5)$$

where $Q_e$ and $Q_t$ are the amount of TCP adsorbed onto adsorbents ($mg \cdot g^{-1}$) at equilibrium and at time t (min), respectively. $k_1$ ($min^{-1}$) and $k_2$ ($g \cdot mg^{-1} \cdot min^{-1}$) are the rate constants of pseudo-first and pseudo-second order models, respectively.

The results were also listed in **Table 2**. It was found that the correlation coefficients of pseudo-second order model for GO sheets and GO sponge were both near to 1.0. It could be inferred that chemical adsorption may be involved in the adsorption process. The strong adsorption of hydroxyl-substituted TCP indicated that its adsorption reaction was related to the presence of hydroxyl group. It was well known that GO has less p-electron and more O-containing groups on its surface. Thus, hydroxyl groups of TCP could interact with O-containing groups on GO through hydrogen-bonding interactions.

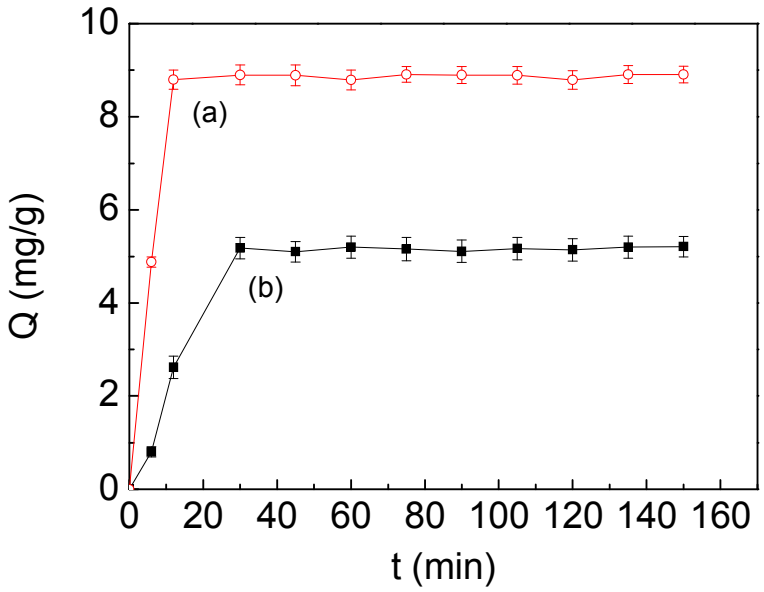


**Fig. 10** Adsorption kinetics of TCP on GO sheets (a) and GO sponge (b)

| Adsorbents | Pseudo first-order model | | Pseudo second-order model | |
|---|---|---|---|---|
| | $k_1$ ($min^{-1}$) | $R^2$ | $k_2$($mg \cdot g^{-1} \cdot min^{-1}$) | $R^2$ |
| **GO sheets** | 0.042 | 0.901 | 0.1186 | 0.985 |
| **GO sponges** | 0.15 | 0.944 | 0.322 | 0.997 |

**Table 2** Adsorption kinetic parameters of TCP on GO sheets and GO sponge

## 4. Conclusions

In this study, GO sponge as novel adsorbents had successfully been prepared via freeze-drying process. Spongy and foam-like structure of GO sponge was endowed with ultralarge surface areas and showed better adsorption capacity of TCP than GO sheets due to more sufficient and stronger hydrogen-bonding interactions of oxygen-containing functional groups on the surface. The results suggest that TCP had

optimum adsorption capacity on both GO sheets and GO sponge at pH 2.0~6.0. Adsorption isotherms and kinetics curves of TCP on GO sheets and GO sponge were nonlinear, indicating the homogeneous monolayer chemical adsorption. In other words, except for hydrophobic interaction, hydrogen-bonding interactions were involved in adsorption. Therefore, GO sponge could be considered as an excellent and economical adsorption material for the removal of pollutants.

## Acknowledgements

The authors gratefully acknowledge financial support from Ministry of Science and Technology of China (Grants Nos. 2012AA03A602 and 2012AA021505), the Key Laboratory of Marine Chemistry Theory and Technology, Ministry of Education (No. 841313040) and Shandong Major Project of Science and Technology (2012CX7301).

## References

1. G.-C. S. Chen, Xiao-Quan; Wang, Yu-Sheng; Wen, Bei; Pei, Zhi-Guo; Xie, Ya-Ning; Liu, Tao; Pignatello, Joseph J., *Water Research*, 2009, **43**, 10.
2. J. Z. Fan, Jian; Zhang, Chenglu; Ren, Liang; Shi, Qianqian, *Desalination*, 2011, **267**, 8.
3. Y. Ide, Y. Nakasato and M. Ogawa, *Journal of the American Chemical Society*, 2010, **132**, 3601-3604.
4. W. Chen, L. Duan, L. Wang and D. Zhu, *Environmental science & technology*, 2008, **42**, 6862-6868.
5. P. Zuman and J. Ludvík, *Electroanalysis*, 2000, **12**, 879-888.
6. K. S. Novoselov, A. K. Geim, S. V. Morozov, D. Jiang, Y. Zhang, S. V. Dubonos, I. V. Grigorieva and A. A. Firsov, *Science*, 2004, **306**, 666-669.
7. D. A. Dikin, S. Stankovich, E. J. Zimney, R. D. Piner, G. H. Dommett, G. Evmenenko, S. T. Nguyen and R. S. Ruoff, *Nature*, 2007, **448**, 457-460.
8. Y. Gao, Y. Li, L. Zhang, H. Huang, J. Hu, S. M. Shah and X. Su, *J Colloid Interface Sci*, 2012, **368**, 540-546.
9. T.-Y. Lin and D.-H. Chen, *RSC Advances*, 2014.
10. G. Zhao, J. Li, X. Ren, C. Chen and X. Wang, *Environmental science & technology*, 2011, **45**,

10454-10462.
11. V. Chandra and K. S. Kim, *Chemical Communications*, 2011, **47**, 3942-3944.
12. K. Yang and B. Xing, *Chemical reviews*, 2010, **110**, 5989-6008.
13. M. Şinoforoğlu, B. Gür, M. Arık, Y. Onganer and K. Meral, *RSC Advances*, 2013, **3**, 11832-11838.
14. C. Gómez-Navarro, J. C. Meyer, R. S. Sundaram, A. Chuvilin, S. Kurasch, M. Burghard, K. Kern and U. Kaiser, *Nano letters*, 2010, **10**, 1144-1148.
15. H. Bi, X. Xie, K. Yin, Y. Zhou, S. Wan, L. He, F. Xu, F. Banhart, L. Sun and R. S. Ruoff, *Advanced Functional Materials*, 2012, **22**, 4421-4425.
16. F. Liu, S. Chung, G. Oh and T. S. Seo, *ACS applied materials & interfaces*, 2012, **4**, 922-927.
17. M. Torkar, V. Leskovšek, B. Šuštaršič and P. Panjan, *Engineering Failure Analysis*, 2002, **9**, 213-219.
18. H. Kamiya, K. Isomura, G. Jimbo and T. Jun‐ichiro, *Journal of the American Ceramic Society*, 1995, **78**, 49-57.
19. B. Jodoin, *Thermal Spray 2001: New Surfaces for a New Millennium*, 2001, 9.
20. D. Z. Fukasawa T, Ando M, Ohji T, Goto Y, *J Mater Sci*, 2001, **36**, 7.
21. W. Li, K. Lu and J. Walz, *International Materials Reviews*, 2012, **57**, 37-60.
22. H. Sun, Z. Xu and C. Gao, *Advanced Materials*, 2013, **25**, 2554-2560.
23. K. Lu, C. S. Kessler and R. M. Davis, *Journal of the American Ceramic Society*, 2006, **89**, 2459-2465.
24. D. C. Marcano, D. V. Kosynkin, J. M. Berlin, A. Sinitskii, Z. Sun, A. Slesarev, L. B. Alemany, W. Lu and J. M. Tour, *ACS nano*, 2010, **4**, 4806-4814.
25. S. Yang, W. Yue, D. Huang, C. Chen, H. Lin and X. Yang, *RSC Advances*, 2012, **2**, 8827-8832.
26. G. Eda and M. Chhowalla, *Adv Mater*, 2010, **22**, 2392-2415.
27. K. N. Kudin, B. Ozbas, H. C. Schniepp, R. K. Prud'Homme, I. A. Aksay and R. Car, *Nano letters*, 2008, **8**, 36-41.
28. W. S. Choi, S.-H. Choi, B. Hong, D.-G. Lim, K.-J. Yang and J.-H. Lee, *Materials Science and Engineering: C*, 2006, **26**, 1211-1214.
29. D. R. Dreyer, S. Park, C. W. Bielawski and R. S. Ruoff, *Chemical Society Reviews*, 2010, **39**, 228-240.
30. V. H. P. Thuy-Duong Nguyen-Phan, Eun Woo Shin[a], Hai-Dinh Pham, Sunwook Kim,Jin Suk Chung, Eui Jung Kim, Seung Hyun Hur, *Chemical Engineering Journal*, 2011, **170**, 7.
31. Z. Pei, L. Li, L. Sun, S. Zhang, X.-q. Shan, S. Yang and B. Wen, *Carbon*, 2013, **51**, 156-163.
32. G. Zhao, L. Jiang, Y. He, J. Li, H. Dong, X. Wang and W. Hu, *Advanced Materials*, 2011, **23**, 3959-3963.